Published in final edited form as:
J Comput Aided Mol Des. 2006 ; 20(0): 405–416. doi:10.1007/s10822-006-9053-3.

Dynamic models of G-protein coupled receptor dimers: indications of asymmetry in the rhodopsin dimer from molecular dynamics simulations in a POPC bilayer

Marta Filizola,
Department of Physiology & Biophysics, Weill Medical College of Cornell University, 1300 York Ave, New York, NY 10021, USA

Simon X. Wang, and
Department of Physiology & Biophysics, Weill Medical College of Cornell University, 1300 York Ave, New York, NY 10021, USA

Harel Weinstein
Department of Physiology & Biophysics, Weill Medical College of Cornell University, 1300 York Ave, New York, NY 10021, USA. HRH Prince Alwaleed Bin Talal Bin Abdulaziz Alsaud Institute for Computational Biomedicine, Weill Medical College of Cornell University, 1300 York Ave, New York, NY 10021, USA

Marta Filizola: maf2037@med.cornell.edu; Harel Weinstein: haw2002@med.cornell.edu

Abstract

Based on the growing evidence that G-protein coupled receptors (GPCRs) form homo- and hetero-oligomers, models of GPCR signaling are now considering macromolecular assemblies rather than monomers, with the homo-dimer regarded as the minimal oligomeric arrangement required for functional coupling to the G-protein. The dynamic mechanisms of such signaling assemblies are unknown. To gain some insight into properties of GPCR dimers that may be relevant to functional mechanisms, we study their current structural prototype, rhodopsin. We have carried out nanosecond time-scale molecular dynamics (MD) simulations of a rhodopsin dimer and compared the results to the monomer simulated in the same type of bilayer membrane model composed of an equilibrated unit cell of hydrated palmitoyl-oleoyl-phos-phatidyl choline (POPC). The dynamic representation of the homo-dimer reveals the location of structural changes in several regions of the monomeric subunits. These changes appear to be more pronounced at the dimerization interface that had been shown to be involved in the activation process [Proc Natl Acad Sci USA 102:17495, 2005]. The results are consistent with a model of GPCR activation that involves allosteric modulation through a single GPCR subunit per dimer.

Keywords

GPCRs; Dimerization; Allosteric mechanism; Dynamic mechanisms; Membrane bilayer; Essential dynamics; GROMACS

Correspondence to: Marta Filizola, maf2037@med.cornell.edu; Harel Weinstein, haw2002@med.cornell.edu.

Introduction

The growing understanding of the signaling mechanism of G protein-coupled receptors (GPCRs) has been complicated recently by compelling evidence that these receptors can be organized in the cell membrane as homo- or hetero-oligomers [1–7]. As it becomes clearer that such oligomeric structures are important for activation [8] and have physiological relevance [9] functional models of GPCR dimers/oligomers are needed to characterize the structural context of receptor association, and its implication in receptor function.

Recent results from Palczewski's lab [10, 11] have suggested that a dimer, or even a larger oligomer, is involved in the functional coupling of rhodopsin to the hetero-trimeric G-protein transducin. Although monomers of rhodopsin are capable of activating transducin, the dimeric form of this prototypic GPCR has been shown to couple the G-protein more efficiently [12]. Using data from atomic force microscopy maps of rhodopsin in its native disk membrane [13] together with information from the receptor crystal structure [14], Palczewski's lab proposed the first three-dimensional molecular model of a rhodopsin oligomer [11]. This model showed a macromolecular arrangement of rhodopsin molecules into two dimensional arrays of dimers involved in both intra-dimeric interactions through transmembrane (TM) helices 4 and 5 (TM4 and TM5), and inter-dimeric interactions of TM1, TM2, and the cytoplasmic loop connecting TM5 and TM6. Results from a very short unconstrained 500 ps molecular dynamics (MD) simulation of this model embedded in a lipid bilayer agreed with the intra-dimeric distances between the rhodopsin monomers determined in the paracrystal [10]. Interestingly, recent cross-linking studies of opsin molecules in COS1 cells [15] confirmed Palczewski's TM4,5–TM4,5 dimer interface by showing that amino acids at the dimer interface of opsin molecules include residuesW175 and Y206, which are present on the extracellular loop connecting TM4 and TM5, and on the extracellular side of TM5, respectively.

Even with this oligomeric geometry as a reasonable form of GPCR association (at least for rhodopsin), it is still unclear whether both monomers in a dimer would be turned on for signal transduction, or whether one activated subunit is sufficient to activate the G-protein. If there is asymmetry in the activation process, it is also a question whether all GPCRs undergo trans-activation so that ligand-binding to one dimeric subunit affects the conformation of the unliganded subunit, which then couples to the G-protein. Several experimental observations (recently reviewed in [6]) are consistent with the possibility of asymmetric functioning for various members of the GPCR superfamily, including rhodopsin. In fact, since a single photon can be detected by the retina [5], one rhodopsin molecule would be sufficient to activate the G-protein. Asymmetric functioning has been demonstrated for Class C GPCRs, such as the γ-aminobutyric acid B ($GABA_B$) receptors and the metabotropic glutamate receptors (mGluRs). These receptors are considered prototypical dimeric receptor models as their functional unit consists of constitutive dimers [16]. The $GABA_{B(1)}$–$GABA_{B(2)}$ hetero-dimer provides the most unequivocal evidence for a GPCR dimer functioning via trans-activation: one ligand-bound subunit is not capable of G-protein coupling, whereas the other subunit within the hetero-dimer can bind the G-protein, but not the ligand [17–19]. The asymmetric interaction between the hetero-trimeric G-

protein and a symmetric GPCR dimer proposed recently from molecular modeling studies [10] constitutes an attractive explanation for the loss of symmetry in a GPCR homo-dimer [20, 21]. However, experimental data on GPCR dimers in their physiological settings, i.e. in the presence of G proteins, are still required to settle this issue.

Reviews and compendia of results from both experimental and computational studies (e.g., see [22, 23] for recent reviews) have discussed fundamental questions regarding the molecular and structural requirements for GPCR function. More often than not, the activation mechanism of a GPCR has been associated with dynamic changes in the monomer, with the most established conformational change involving TM6 and its movement away from TM3 in the cytoplasmic end of the TM bundle. For the dopamine D2 receptor more recent data [8] demonstrated that a rearrangement of the dimer interface is a critical component of the activation mechanism. This inference is based on the observation that the susceptibilities to crosslinking of cysteine mutants at the homodimer interface are differentially altered by agonists and inverse agonists. In particular, in the inverse agonist-bound conformation, the TM4 dimer interface is consistent with the dimer model of the inactive form of rhodopsin [11]. On the other hand, agonists accelerate crosslinking of a different set of loci on the TM4 face, and diminish crosslinking on the interface preferred by the inverse agonist [8]. These results indicate that the TM4 interface changes upon activation. Because all these models are based on the structure of rhodopsin, we focus here on the structure of rhodopsin and its dimer model to explore the specifics of the interface dynamics that could be involved in functional signaling. Results from MD simulations of the molecular model of a rhodopsin dimer are compared to corresponding findings for the monomer. We present the results from the first 45 ns of MD simulations of a TM4,5–TM4,5 configuration of the rhodopsin dimer, and of the monomer, in an equilibrated rectangular unit cell of a hydrated palmitoyl-oleoyl-phosphatidyl choline (POPC) bilayer membrane. An essential dynamics analysis of these results reveals specific positions in the dimer where the intrinsic asymmetry of the system is accentuated. This includes the dimerization interface. The pattern of structural flexibility of the dimer model revealed from these MD simulations is in line with the hypothesis suggested by our recent results from a combined experimental and modeling study [8] that a conformational rearrangement of the dimerization interface may be an important part of the allosteric modulation of GPCR function.

Methods

Molecular systems

A refined molecular model of the inactive rhodopsin monomer was constructed using the rhodopsin crystal structure corresponding to the Protein Data Bank (PDB) identification (ID) code 1L9H [24] as a template, and two powerful techniques that have been developed in our laboratory. Specifically, an ab-initio method that has been demonstrated to predict the conformations of large loop regions reliably [25–27] was used to build the cytoplasmic loop fragments (amino acids 236–240 and 331–333) that were missing in the 1L9H crystal structure [24]. The proposed conformations of these fragments were found to be consistent with the ones solved in the latest crystal structure of bovine rhodopsin (PDB ID code: 1U19) [28]. In addition, a microenvironment modulated-screened Coulomb potential approach to

calculate pK_a values was used to assign accurate protonation states to the titratable groups of rhodopsin [29]. Furthermore, a Grand Canonical Ensemble Metropolis Monte Carlo (MMC) cavity biased insertion method [30], which has been demonstrated to be successful in determining water positions in a number of crystal structures [31, 32], was used to find optimal placement of internal water molecules in rhodopsin. Using this method, which improves statistical sampling efficiency, 72 internal water molecules were placed in the refined structure of the rhodopsin monomer. This number of water molecules is higher than the number found in published rhodopsin crystal structures [24, 28]. Yet, the excess of water molecules was found in the proximity of the intracellular loop region, which is technically not an “internal” region.

Among all heteroatoms in the monomeric crystal structure (*N*-acetyl-D-glucosamine, α-D-mannose, B-nonylglucoside, heptane-1,2,3-triol, metal ions Hg^{2+} and Zn^{2+}), only covalently bound molecules were included in the simulations. Specifically, the ligand retinal, which is covalently bound to the receptor Lys296 via a protonated Schiff base, and palmitoyl chains, which are covalently bound to rhodopsin residues Cys322 and Cys323, were taken into account. Parameters for palmitoyl chains were adopted from the GROMACS force field [33, 34], which is based on the GROMOS-87 force field. Parameters for the retinal were taken from previous studies [35–38] and adjusted to GROMACS force field. For the rhodopsin dimer, an initial model was obtained by overlapping the refined inactive monomeric structure of rhodopsin [27] including the optimal protonation state [29] and 72 internal water molecules, onto the rhodopsin dimer model with TM4 and TM5 at the interface (PDB ID code: 1N3M) [11].

An explicit membrane-explicit water environment was considered in the simulations of both rhodopsin monomer and dimer. Hydrated palmitoyl-oleoyl-phosphatidyl choline (POPC) bilayer unit cells that could accommodate the initial configurations of the rhodopsin monomer and dimer were generated by duplicating and truncating a fully pre-equilibrated 8 × 8 × 2 POPC patch [39, 40]. Specifically, a hydrated POPC bilayer tetragonal unit cell (a = b = 112 Å, c = 98 Å) composed of 352 lipid molecules and 23,318 water molecules was built for the rhodopsin monomer. The rhodopsin dimeric model was embedded in a hydrated POPC bilayer orthorhombic unit cell (a = 160 Å, b = 124 Å, c = 98 Å) with 567 lipid molecules and 35,852 water molecules. The size of these unit cells was determined by considering a minimum of four layers of lipid molecules around the protein, which resulted in a minimum distance of 20 Å between periodic images of the solute. We had previously shown these settings to be appropriate for protein–lipid simulations [41–43]. Finally, one Na^+ ion was added to neutralize each monomer.

After solvent equilibration (see following section for details), the initial monomeric and dimeric rhodopsin structures were placed in the hydrated POPC bilayer unit cells using inferences from both computational and experimental studies on GPCRs (for reviews see [44, 45]). Specifically, the TM4 helical axis was imposed to be normal to the membrane plane. This particular placement of TM4 determined helix 8 lying at the hydrophobic/hydrophilic interface of the POPC bilayer and the side chains of its polar residues (Lys311, Gln312, Arg314, Asn315 and Thr319) pointing toward the water phase. Finally, the highly conserved R134 of the D/ERY motif, as well as its interacting TM6 partner E247 were

found to be surrounded by lipid headgroups. After superposition of lipid patch and protein, lipids clashing with the protein were removed, whereas the rest of them was subjected to equilibration and optimal arrangement around the protein.

Molecular dynamics simulations

MD simulations of both rhodopsin monomer and dimer in explicit lipid–water environments were performed in the NPT ensemble (constant pressure and temperature) and periodic boundary conditions using the GROMACS program package [33, 34]. Lipid parameters were taken from Berger et al. [46] and Simple Point Charge (SPC) water molecules were chosen as water model. Coulomb and short-range neighbor list cutoffs were both set to 0.9 nm, whereas the Lennard–Jones cut-off was set to 1.2 nm. Electro-static contributions to the energies and forces were calculated using the Particle-Mesh Ewald (PME) summation algorithm [47]. The interpolation order was set to 6 and the maximum spacing for the combined charge/potential grid was set to 0.12 nm. Sodium counterions (1 Na^+ for the monomeric system and 2 Na^+ for the dimer) were used to replace water molecules at positions of the strongest negative electro-static potential, thus obtaining electrically neutral systems. A time step of 2 fs, and the pair lists were updated every 10 steps. The LINear Constraint Solver (LINCS) algorithm [48] was used to preserve the bond lengths. The weak-coupling scheme proposed by Berendsen [49] was used for temperature and pressure control. Specifically, a temperature of 310 K was maintained constant with a time constant of 0.1 ps. For the pressure, semi-isotropic coupling was used with the reference pressure set at 1.0 bar.

Analysis of the trajectories

To assess the stability of the simulations, several geometrical properties (e.g., radius of gyration, total number of hydrogen bonds, root mean square displacement, solvent accessibility) were monitored using GROMACS routines. To compare the conformational subspaces of each subunit of the dimer with one another as well as with the rhodopsin monomer, a Combined Essential Dynamics (Comb-ED) analysis [50] was performed. Essential dynamics analysis separates the configurational space into an essential subspace with a few degrees of freedom which describe overall motions of the protein that are likely to be relevant to its function, and a physically constrained subspace describing local fluctuations. The method is based on the diagonalization of the covariance matrix of atomic fluctuations defined by:

$$C_{ij}=\langle (x_i-\langle x_i\rangle)\,(x_j-\langle x_j\rangle)\rangle \quad (1)$$

where x_i are the three Cartesian coordinates of the carbon atoms Cα of the molecule under study, and $\langle\ \rangle$ are averages over an ensemble of configurations from the time-interval of the MD simulation for which the system is stable. The diagonalization of Eq. (1) yields eigenvectors that describe the directions of correlated positional changes in the molecule, whereas the eigenvalues indicate the total mean square fluctuation along these directions. The hypothesis is that only the eigenvectors with large corresponding eigenvalues (by convention, the first eigenvectors) are important in describing the overall motion of a protein.

In the Comb-ED, the covariance matrix is calculated for two or more concatenated trajectories, which have been fitted on the same reference structure. Given this construct, the eigenvectors resulting from Comb-ED do not represent the essential degrees of motion of the molecules, but they reveal differences and similarities in the dynamical and structural characteristics of the compared simulated structures. To identify structural differences between the two subunits of the dimer, as well as between each dimer subunit with the rhodopsin monomer, we concatenated the last 17.5 ns of the compared trajectories in the following pairings: the last 17.5 ns of subunit A with subunit B, the last 17.5 ns of subunit A with the monomer, and of subunit B with the monomer.

Large-scale dynamic rigid body motions were analyzed using in-house computational tools such as Prokink [51] for the calculation of helical kink values, and TRAJELIX [52] for a comprehensive geometric characterization of protein helices during molecular dynamics simulations.

Results and discussion

The results of the first 45 ns of MD simulations of a dimer of the prototypic GPCR rhodopsin are presented in comparison to the outcomes from analogous simulations of the rhodopsin monomer. Results of several simulations of rhodopsin monomer in realistic explicit membrane environments are available in the literature [53–58] and are comparable to our monomer simulations, but to the best of our knowledge, this is the first time an extensive MD simulation is presented for a GPCR dimer in an explicit water–lipid environment.

Environment

A hydrated patch of POPC lipid bilayer was used here to simulate the membrane environment of rhodopsin, in both its monomeric and dimeric forms. This constitutes a simplified model of rhodopsin's physiological environment that comprises a variety of unsaturated lipids residing in the disk membranes of rod cells, but experiments have shown that rhodopsin reconstituted in artificial membranes is also functional [59]. The lipid unit cells for the rhodopsin monomer and dimer were different in size, but were both constructed by duplicating and truncating Thielman's equilibrated 8 × 8 × 2 POPC patch [39, 40]. Based on the dimensions of a rhodopsin monomer (44 × 46 Å) as calculated from PDB 1L9H, a lipid unit cell containing 14 × 14 × 2 POPC molecules was built to contain the protein monomeric form. Similarly, an average size of 85 × 50 Å for the rhodopsin dimer—as calculated from the oligomeric complex recently proposed by Liang et al. (PDB ID code: 1N3M)—suggested the construction of a lipid unit cell containing 20 × 16 × 2 POPC molecules. Pre-equilibrated water molecules were then added at the edges of both lipid patches in the direction of the membrane normal, and several cycles of steepest descent minimization followed by conjugate gradient minimization were performed to minimize the energy of each system until a convergence of 100 kJ mol^{-1} nm^{-1} was achieved.

To achieve stability of the lipid environment during unrestrained MD simulations, 2 ns equilibration MD runs were performed for both the hydrated POPC unit cells built for the rhodopsin monomer and dimer until lipid properties such as order parameter and area per

lipid were converged to the experimental values. Indeed, the potential energy of the system reached a stable plateau after 1 ns simulation time (see Fig. 1a for the dimer lipid cell), the temperatures remained at 310 K for the 2 ns simulation (Fig. 1b), and the area of the *xy* plane per lipid (Fig. 1c) fluctuated around 61.8 $Å^2$, which is close to the value found experimentally [60]. The deuterium order parameter profile taken over the last 1 ns of the trajectories (shown in Fig. 1d for the hydrated lipid cell that would accommodate the rhodopsin dimer) was also consistent with the experimental data [60].

Overall structural stability

After equilibration of their respective hydrated membrane patches, the rhodopsin monomer and dimer systems were each embedded in the corresponding membrane patch according to an optimal matching of the protein's hydrophobic and hydrophilic surfaces with the hydrophobic and hydrophilic parts of the solvent unit cells (see Methods section for details). After neutralizing the net charge of the unit cells with sodium ions, the monomeric and dimeric systems contained 92,057 and 144,638 atoms, respectively. Figure 2 shows the initial rhodopsin dimer/membrane/water system in its orthogonal unit cell.

Simulations were run for 45 ns, and their stability was checked by monitoring several time-dependent geometrical properties. Among them, Fig. 3 reports the root mean-square deviations (RMSD) of the Cα atoms of the entire dimer (black line) and each of its two subunits (dark gray for subunit A and light gray for subunit B) from the starting structure. As shown in this figure, the whole dimer, as well as the two individual subunits, appear to have reached equilibration after 27.5 ns. In the last 17.5 ns of simulation, the RMSD of the whole dimer (~3.9 Å) is larger than the RMSD observed for subunit A (~3.2 Å) and subunit B (~2.6 Å), suggesting a rearrangement of the protein quaternary structure during the simulation (see following section). In addition, one of the two subunits (A) appears to deviate more than the other from the initial structure, suggesting different changes within each monomer. Yet, the simulated systems maintain their global folding, as indicated by the time evolution of their secondary structure elements, the total number of hydrogen bonds, the radius of gyration of the Cα atoms, and the total accessible surface area (data not shown).

Rearrangement of the dimer quaternary structure

A rough estimate of the rearrangement of the protein quaternary structure during the 45 ns MD simulation is given by the distances between the centers of mass of the TM4 or TM5 helices at the interface of the rhodopsin dimer plotted as a function of time (Fig. 4). The distance between TM4 helices becomes ~2 Å shorter after equilibration, remaining stable at ~14 Å afterwards. Thus, in long time-scale simulations the TM4–TM4 interface of the rhodopsin dimer becomes more compact than has previously been suggested [10, 11]. Interestingly, as the TM4 helices come closer together, the TM5 helices become separated by an equivalent distance (~2 Å).

The Cα atom RMSD between the structure at the end of the equilibrated portion of the trajectory and the initial structure is 3.7 Å. However, separate superpositions of the two subunits of the dimer yield lower RMSDs. Specifically, subunits A and B deviate 3.2 and

2.6 Å, respectively, from their initial structures. Using the DynDom Protein Domain Motion Analysis program [61] we calculated that when the subunit B of the final structure is superimposed onto its initial structure, subunit A must rotate 16° to best fit the initial conformation.

Differences in the conformational spaces of the dimer subunits

Not surprisingly, the root mean square fluctuation (i.e. standard deviation) of the Cα atomic positions of each subunit of the dimer after fitting to their individual initial structures shows that the loop regions of the protein move the most during the molecular dynamics simulation. The specifics evident in Fig. 5 are that the largest deviations from the initial structures of both subunits is in the N-terminus (residues 1–34), the intracellular loop (IC) between TM3 and TM4 (IC2, residues 140–150), the intracellular loop between TM5 and TM6 (IC3, residues 226–246), and the C-terminus (residues 322–348). Although the deviation pattern is very similar in the two subunits, significant differences exist between them. Specifically, subunit A (black line in Fig. 5) appears to have changed more than subunit B (gray line in Fig. 5) in the N- and C-termini, and in the regions 75–125 (including: TM2, the extracellular loop 1 (EL1), and TM3), and 151–175 (corresponding to TM4).

To compare the conformational spaces of the two subunits of the rhodopsin dimer during the MD simulations, we carried out a type of essential dynamics analysis termed Comb-ED (see Methods section). This particular type of essential dynamics analysis is based on the diagonalization of the covariance matrix of atomic fluctuations taken from concatenated stable trajectory intervals (in this case the last 17.5 ns of the trajectories of both subunits A and B); it has been shown to be particularly efficient in comparing two or more conformational states of the same protein [50]. Figure 6a shows that the first eigenvector resulting from diagonalization of the covariance matrix of atomic fluctuations describes the principal structural differences between the conformational spaces of the two subunits of the dimer. As shown in Fig. 6b, these differences involve the same regions as those revealed by the positional root mean square fluctuations shown in Fig. 5, i.e. the N- and C-termini, the TM2-EL1-TM3 region and the TM4 helix at the dimerization interface.

Comparison of the conformational spaces of each dimeric subunit with the monomer

Comb-ED was also used to assess the nature and location of differences and similarities between the conformational spaces of each subunit of the dimer and the rhodopsin monomer. Figure 7a describes the differences encoded by the first eigenvector between the transmembrane regions of subunit A in the dimer and the rhodopsin monomer. Figure 7b shows the same comparison for subunit B of the dimer and the monomer. The differences between the dynamics of the two subunits of the rhodopsin dimer are evidenced by the comparison to the monomer in these Figures. For subunit A of the dimer (Fig. 7a) and the monomer, these differences appear to be larger than those between subunit B of the dimer and the monomer. Specifically, the TM4 and TM2 regions of subunit A of the dimer seem to have diverged more from the monomer than the same regions of subunit B.

Large-scale rigid body motions

Large-scale rigid body motions (e.g., the motion of TM6 relative to TM3 [62], the motion of TM4 [63], etc.) have been suggested to play a key role in the activation mechanism of GPCRs. More recently, the activation was shown to involve changes at the dimer interface [8]. Although no activation could possibly be achieved during these first 45 ns of MD simulation of the rhodopsin dimer, the intriguing suggestion of different large-scale rigid body motions within the two subunits of the rhodopsin dimer warranted detailed analysis. This analysis included calculations of total helix tilt angles, rotations around helical axes, and the dynamic behavior of helix kinks.

Figure 8 shows the time evolution (recorded every 10 ps) of the total tilt angle of each TM of rhodopsin with respect to the *Z*-axis (or bilayer normal) during the 45 ns of MD simulation. The pairwise comparison of total tilt angles calculated for individual helices of the two subunits A and B of the dimer (shown in dark gray and light gray, respectively, in Fig. 8) over the last 17.5 ns production run time shows slight differences, ranging from a minimum value of 5° to a maximum of 10°. Notably, the TM5 helices at the dimer interface differ the most in total tilt values. Interestingly, unlike the situation for subunit A of the dimer, the total tilt of TM5 calculated for the subunit B of the rhodopsin dimer (in light gray in Fig. 8) during the stable interval from 27.5 to 45 ns diverge from the TM5 total tilt value calculated for the rhodopsin monomer (black in Fig. 8), indicating a key structural change involved in the observed differences within the dimer.

As rigid body rotations of TM helices have been suggested to play key roles in the activation mechanism of GPCRs (e.g., rotation of TM4 [63]), we also monitored the rotation of each TM around its own helical axis. Helices rotate up to 10° around their own helical axes during the 45 ns MD simulation, with the highest differences between the subunits of the dimer (dark gray and light gray in Fig. 9) recorded for TM1, TM2, and TM6. Interestingly, the rotation of the TM helices in the rhodopsin monomer (black in Fig. 9) usually differs from those recorded for either of the two subunits of the dimer.

Figure 10 shows the results obtained from calculation of the kink (extent of helical bending) of TM helices of the rhodopsin monomer (black line in the figure) or dimer (dark gray and light gray colors for subunits A and B, respectively). The kinks are caused either by a proline residue or two consecutive glycines, at P53 (1.48), G89 (2.56), G120 (3.35), P170 (4.59), P215 (5.50), P267 (6.50), P291 (7.38), and P303 (7.50). Note that residues are numbered according to their positions in the bovine rhodopsin receptor sequence and also relative to the most conserved residue in the TM in which they are located, which is given the position index “50” as described originally [64]. The kink angles fluctuate within the values found in the rhodopsin X-ray crystal structure. These values can vary up to a maximum of 20° between the two subunits of the dimer during the 17.5 ns production run for TM4, TM6, and TM7.

Conclusions

The recent recognition that GPCR dimers/oligomers have specific functional roles in vivo (e.g., see [9]) has prompted a refocusing on the molecular and dynamic properties of

molecular assemblies instead of receptor monomers. The results of the first 45 ns of a MD simulation of a rhodopsin dimer with TM4 and TM5 at the interface, presented here, reveal the location of structural differences within the system, which mostly involve the extracellular and intracellular regions of the subunits of the dimer. Yet, differences have also been observed in the region of the transmembrane helices. Among them, the TM4 helix at the dimerization interface shows the most pronounced structural differences between the two subunits of the rhodopsin dimer. Such differences at the dimer interface upon activation are consonant with the rearrangement of the dimer interface suggested by the data for the cognate dopamine D2 receptor [8].

The observation from combined essential dynamics, that the conformational space of one of the two subunits of the rhodopsin dimer (A) is significantly more different from the conformational space of the monomer dynamics than the other (B), may indicate the nature of allosteric modulation that could connect the monomers in a putative asymmetric activation mechanism of GPCRs. Thus, if GPCR function occurs through activation of a single GPCR subunit per dimer, asymmetric rearrangements will be required for signal transduction. This is consonant with recent data published in the literature providing evidence for asymmetric functioning of several GPCRs (e.g., rhodopsin [12], $GABA_B$ receptors [17–19], metabotropic glutamate receptors [20, 21], etc), which may or may not occur through trans-activation. It is not certain, however, that these rearrangements will be preserved when the GPCR structure in the dimer changes to the activated form. As the simulations were carried out with an inactive conformation of rhodopsin in the dimer, the data shown here may only indicate properties inherent in the receptor molecules and their environment. Consequently, they can only be considered to reflect the possible initial trends of the changes related to activation. To clarify these issues, we are currently constructing models of activated forms of the rhodopsin dimer, to enable comparisons of their dynamics with the structure simulated here. In a study reported elsewhere in this same issue, we present five different active state models of the rhodopsin monomer.

Acknowledgments

We are grateful to Dr. Marc Ceruso for help in setting up the initial dimer simulations, and Dr. Nathalie Basdevant for help with the essential dynamics analysis. This work was supported by NIH grants DA00060, DA012923 (to HW) and DA020032, DA017976 (to MF) from the National Institute on Drug Abuse.

References

1. Terrillon S, Bouvier M. EMBO Rep. 2004; 5(1):30. [PubMed: 14710183]
2. Javitch JA. Mol Pharmacol. 2004; 66(5):1077. [PubMed: 15319448]
3. Milligan G. Mol Pharmacol. 2004; 66(1):1. [PubMed: 15213289]
4. Bai M. Cell Signal. 2004; 16(2):175. [PubMed: 14636888]
5. Park PS, Filipek S, Wells JW, Palczewski K. Biochemistry. 2004; 43(50):15643. [PubMed: 15595821]
6. Filizola M, Weinstein H. Curr Opin Drug Discov Devel. 2005; 8(5):577.
7. Fotiadis D, Jastrzebska B, Philippsen A, Muller DJ, Palczewski K, Engel A. Curr Opin Struct Biol. 2006; 16(2):252. [PubMed: 16567090]
8. Guo W, Shi L, Filizola M, Weinstein H, Javitch JA. Proc Natl Acad Sci USA. 2005; 102(48):17495. [PubMed: 16301531]

9. Waldhoer M, Fong J, Jones RM, Lunzer MM, Sharma SK, Kostenis E, Portoghese PS, Whistler JL. Proc Natl Acad Sci USA. 2005; 102(25):9050. [PubMed: 15932946]
10. Filipek S, Krzysko KA, Fotiadis D, Liang Y, Saperstein DA, Engel A, Palczewski K. Photochem Photobiol Sci. 2004; 3(6):628. [PubMed: 15170495]
11. Liang Y, Fotiadis D, Filipek S, Saperstein DA, Palczewski K, Engel A. J Biol Chem. 2003; 278:21655. [PubMed: 12663652]
12. Jastrzebska B, Maeda T, Zhu L, Fotiadis D, Filipek S, Engel A, Stenkamp RE, Palczewski K. J Biol Chem. 2004; 279(52):54663. [PubMed: 15489507]
13. Fotiadis D, Liang Y, Filipek S, Saperstein DA, Engel A, Palczewski K. Nature. 2003; 421(6919): 127. [PubMed: 12520290]
14. Teller DC, Okada T, Behnke CA, Palczewski K, Stenkamp RE. Biochemistry. 2001; 40:7761. [PubMed: 11425302]
15. Kota P, Reeves PJ, Rajbhandary UL, Khorana HG. Proc Natl Acad Sci USA. 2006; 103(9):3054. [PubMed: 16492774]
16. Pin JP, Kniazeff J, Liu J, Binet V, Goudet C, Rondard P, Prezeau L. Febs J. 2005; 272(12):2947. [PubMed: 15955055]
17. Duthey B, Caudron S, Perroy J, Bettler B, Fagni L, Pin JP, Prezeau L. J Biol Chem. 2002; 277(5): 3236. [PubMed: 11711539]
18. Galvez T, Duthey B, Kniazeff J, Blahos J, Rovelli G, Bettler B, Prezeau L, Pin JP. Embo J. 2001; 20(9):2152. [PubMed: 11331581]
19. Margeta-Mitrovic M, Jan YN, Jan LY. Proc Natl Acad Sci USA. 2001; 98:14643. [PubMed: 11724957]
20. Goudet C, Kniazeff J, Hlavackova V, Malhaire F, Maurel D, Acher F, Blahos J, Prezeau L, Pin JP. J Biol Chem. 2005; 280(26):24380. [PubMed: 15863499]
21. Hlavackova V, Goudet C, Kniazeff J, Zikova A, Maurel D, Vol C, Trojanova J, Prezeau L, Pin JP, Blahos J. Embo J. 2005; 24(3):499. [PubMed: 15660124]
22. Stenkamp RE, Teller DC, Palczewski K. Arch Pharm (Weinheim). 2005; 338(5–6):209. [PubMed: 15952240]
23. Weinstein H. AAPS J. 2006; 7(4):871.
24. Okada T, Fujiyoshi Y, Silow M, Navarro J, Landau EM, Shichida Y. Proc Natl Acad Sci USA. 2002; 99(9):5982. [PubMed: 11972040]
25. Hassan SA, Mehler EL, Zhang D, Weinstein H. Proteins. 2003; 51:109. [PubMed: 12596268]
26. Li XF, Hassan SA, Mehler EL. Proteins Struct Funct Bioinform. 2005; 60(3):464.
27. Mehler EL, Periole X, Hassan SA, Weinstein HJ. Comput Aided Mol Des. 2002; 16(11):841.
28. Okada T, Sugihara M, Bondar AN, Elstner M, Entel P, Buss V. J Mol Biol. 2004; 342(2):571. [PubMed: 15327956]
29. Periole X, Ceruso MA, Mehler EL. Biochemistry. 2004; 43(22):6858. [PubMed: 15170322]
30. Resat H, Mezei M. J Am Chem Soc. 1994; 116:7451.
31. Resat H, Mezei M. Biophys J. 1996; 71(3):1179. [PubMed: 8873992]
32. Marrone TJ, Resat H, Hodge CN, Chang C-H, McCammon JA. Protein Sci. 1998; 7:573. [PubMed: 9541388]
33. Berendsen HJC, van der Spoel D, van Drunen R. Comp Phys Comm. 1995; 91:43.
34. Van Der Spoel D, Lindahl E, Hess B, Groenhof G, Mark AE, Berendsen HJ. J Comput Chem. 2005; 26(16):1701. [PubMed: 16211538]
35. Tajkhorshid E, Baudry J, Schulten K, Suhai S. Biophys J. 2000; 78(2):683. [PubMed: 10653781]
36. Tajkhorshid E, Paizs B, Suhai S. J Phys Chem B. 1997; 101:8021.
37. Tajkhorshid E, Suhai S. J Phys Chem B. 1999; 103:5581.
38. Nina M, Roux B, Smith J. Biophys J. 1995; 68:25. [PubMed: 7711248]
39. Tieleman DP, Berendsen HJ. Biophys J. 1998; 74(6):2786. [PubMed: 9635733]
40. Tieleman DP, Forrest LR, Sansom MS, Berendsen HJ. Biochemistry. 1998; 37(50):17554. [PubMed: 9860871]
41. Sankararamakrishnan R, Weinstein H. Biophys J. 2000; 79(5):2331. [PubMed: 11053113]

42. Sankararamakrishnan R, Weinstein H. J Phys Chem B. 2004; 108:11802.
43. Sankararamakrishnan R, Weinstein H. J Phys Chem B. 2002; 106:209.
44. Visiers I, Ballesteros JA, Weinstein H. Meth Enzymol. 2002; 343:329. [PubMed: 11665578]
45. Fanelli F, De Benedetti PG. Chem Rev. 2005; 105(9):3297. [PubMed: 16159154]
46. Berger O, Edholm O, Jahnig F. Biophys J. 1997; 72:2002. [PubMed: 9129804]
47. Darden T, York D, Pederson L. J Chem Phys. 1993; 98:10089.
48. Hess B, Bekker H, Berendsen HJC, Fraaije JGEM. J Comput Chem. 1997; 18:1463.
49. Berendsen, HJC.; Postma, JPM.; Gunsteren, WF.; Hermans, J. Intermolecular forces. Riedel; Dordrecht: 1981.
50. van Aalten DM, Amadei A, Linssen AB, Eijsink VG, Vriend G, Berendsen HJ. Proteins. 1995; 22(1):45. [PubMed: 7675786]
51. Visiers I, Braunheim BB, Weinstein H. Protein Eng. 2000; 13(9):603. [PubMed: 11054453]
52. Mezei M, Filizola M. J Comp Aid Mol Des. 2006; 20(2):97.
53. Pitman MC, Grossfield A, Suits F, Feller SE. J Am Chem Soc. 2005; 127(13):4576. [PubMed: 15796514]
54. Saam J, Tajkhorshid E, Hayashi S, Schulten K. Biophys J. 2002; 83(6):3097. [PubMed: 12496081]
55. Huber T, Botelho AV, Beyer K, Brown MF. Biophys J. 2004; 86(4):2078. [PubMed: 15041649]
56. Faraldo-Gomez JD, Forrest LR, Baaden M, Bond PJ, Domene C, Patargias G, Cuthbertson J, Sansom MS. Proteins. 2004; 57(4):783. [PubMed: 15317024]
57. Schlegel B, Sippl W, Holtje HD. J Mol Model (Online). 2005; 12(1):49.
58. Crozier PS, Stevens MJ, Forrest LR, Woolf TB. J Mol Biol. 2003; 333(3):493. [PubMed: 14556740]
59. Fong SL, Tsin AT, Bridges CD, Liou GI. Methods Enzymol. 1982; 81:133. [PubMed: 6980357]
60. Petrache HI, Dodd SW, Brown MF. Biophys J. 2000; 79:3172. [PubMed: 11106622]
61. Hayward S, Berendsen HJ. Proteins. 1998; 30(2):144. [PubMed: 9489922]
62. Farrens DL, Altenbach C, Yang K, Hubbell WL, Khorana HG. Science. 1996; 274(5288):768. [PubMed: 8864113]
63. Borhan B, Souto ML, Imai H, Shichida Y, Nakanishi K. Science. 2000; 288(5474):2209. [PubMed: 10864869]
64. Ballesteros JA, Weinstein H. Meth Neurosci. 1995; 25:366.

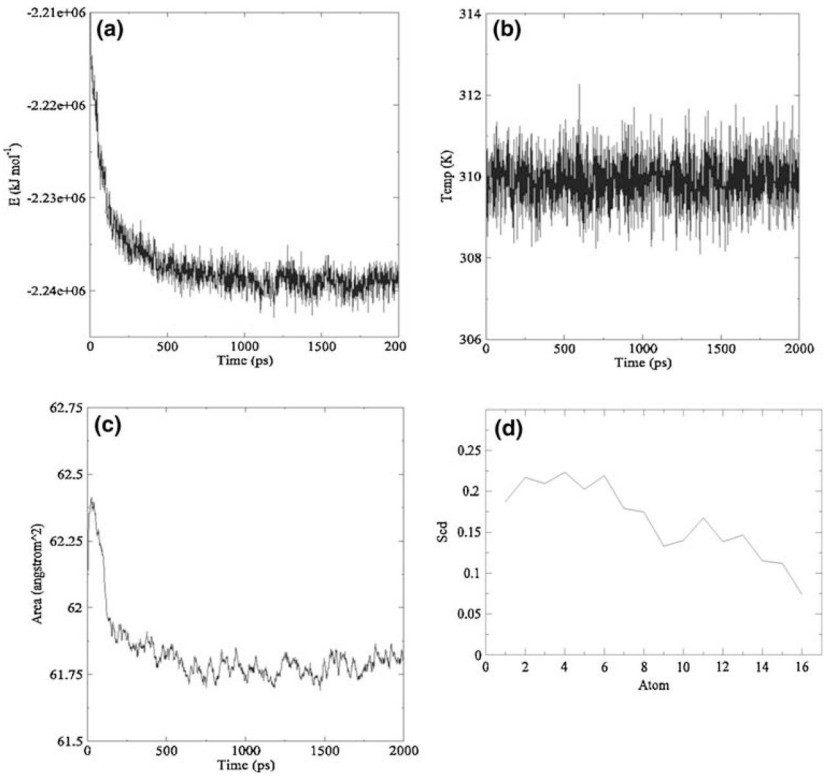

Fig. 1.

Equilibration of the hydrated POPC patch that can accommodate a rhodopsin dimer. Shown as a function of trajectory time are (**a**) the potential energy; (**b**) the temperature of the system; (**c**) the area per lipid in the *xy* plane. The Deuterium order parameter profile is shown in panel (**d**)

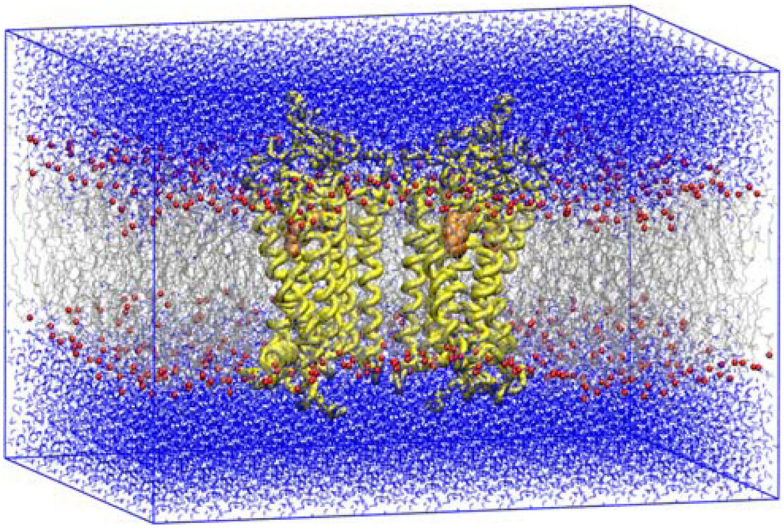

Fig. 2.

Initial structure of the rhodopsin dimer (thick ribbon) in the orthogonal unit cell (solid lines) used to simulate the system with periodic boundary conditions. The view is parallel to the membrane (gray color). The system is solvated in water. The dimer interface is symmetric, and consists of TMs 4 and 5. Molecules of the ligand retinal in the two binding pockets are shown in CPK representations

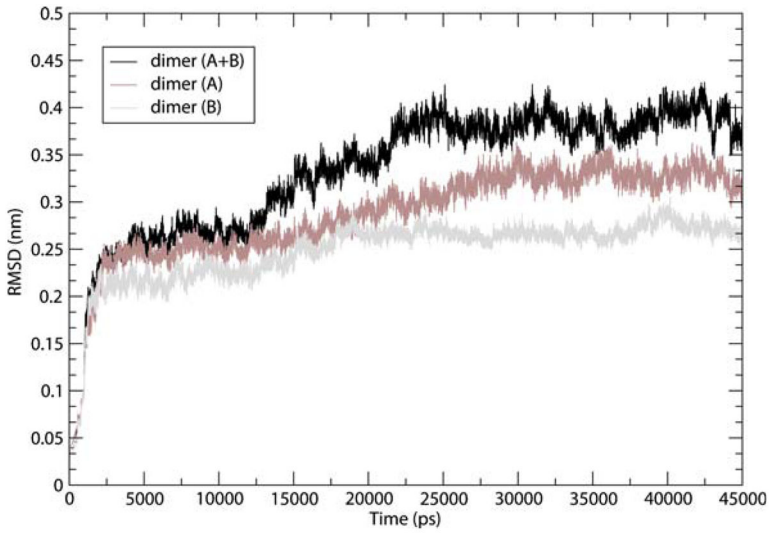

Fig. 3.

Root mean-square deviations from the starting structure calculated for the Cα atoms of the whole dimer (black line) and its subunits A (dark gray line) and B (light gray line)

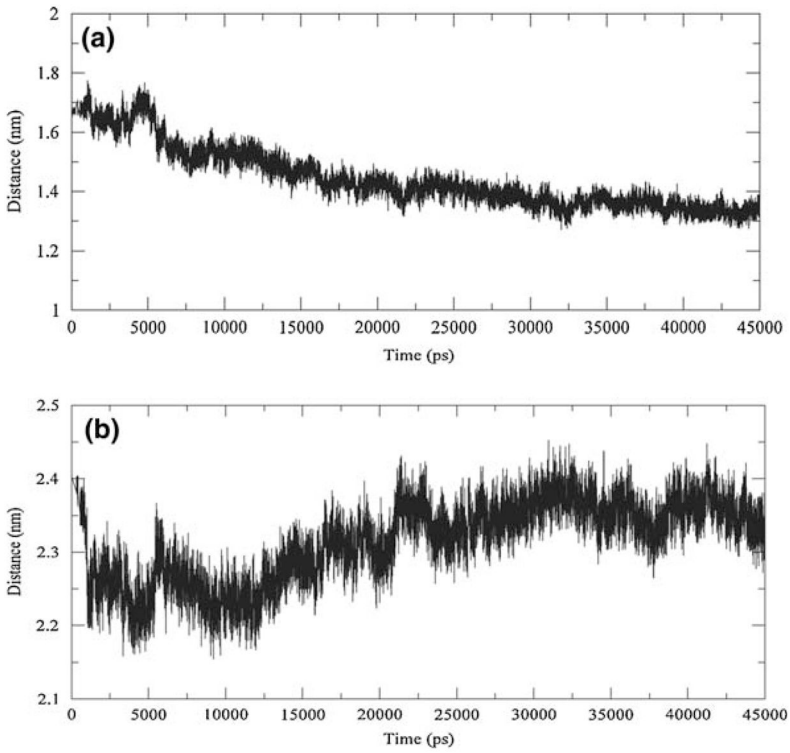

Fig. 4.

Trajectory time evolution of the distances between the centers of mass of the transmembrane helices TM4 (**a**) or TM5 (**b**) at the interface of the rhodopsin dimer

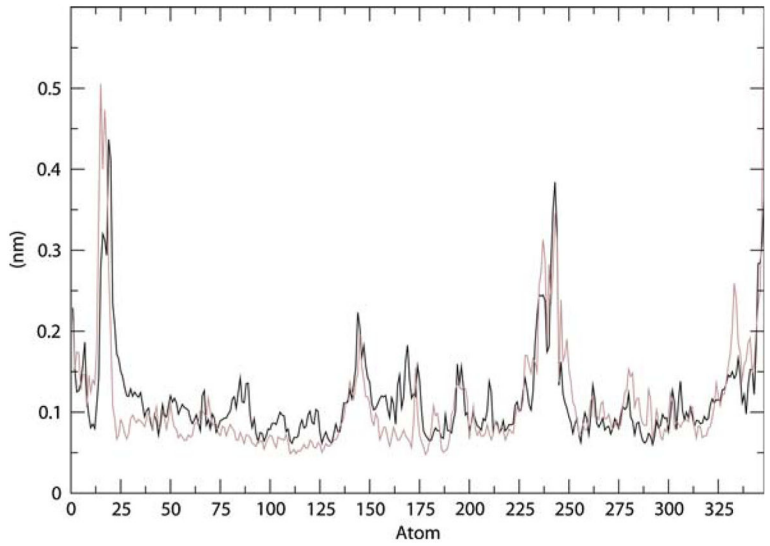

Fig. 5.

Root mean square fluctuation of the Cα atomic positions of subunits A (black line) and B (gray line) of the dimer relative to their individual initial structures

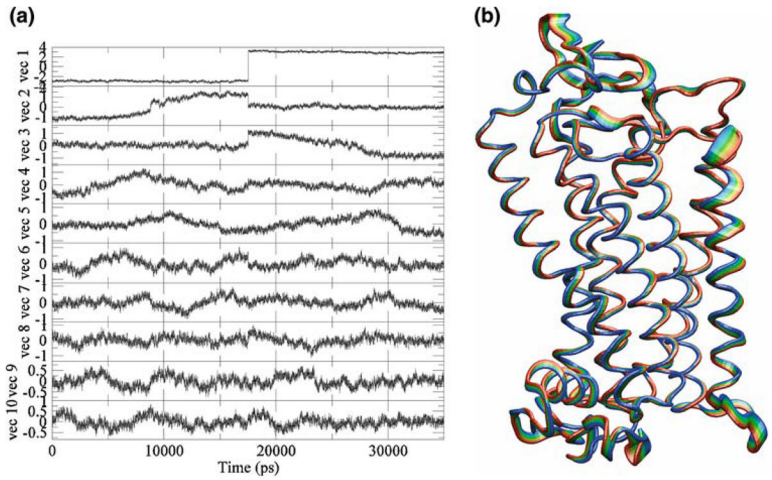

Fig. 6.

Results of the Comb-ED analysis for subunits A and B of the dimer. (**a**) The first 10 eigenvectors resulting from diagonalization of the covariance matrix of atomic fluctuations of the concatenated stable trajectories of A and B. (**b**) Representation of the structural differences between subunits A and B of the dimer: the motions described by the first eigenvector of the Comb-ED are represented by the span of the ribbon diagram, where the structure deviates from the original one as it moves in the direction of the first eigenvector

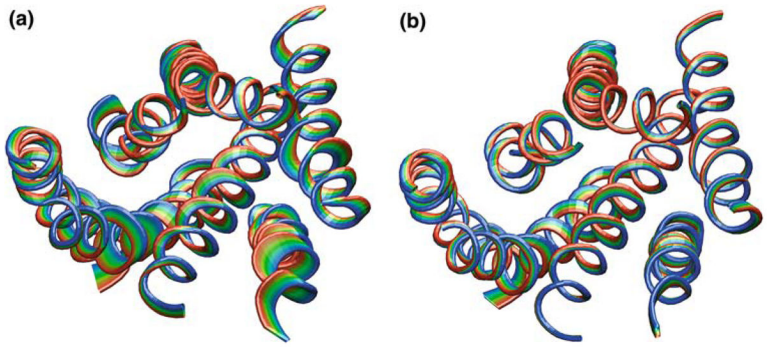

Fig. 7.

Ribbon representation of the structural differences between each subunit of the dimer and the rhodopsin monomer obtained from the Comb-ED analysis (see legend of Fig. 6b for details of the representation). (**a**) Comparison of the transmembrane regions of subunit A in the dimer and the rhodopsin monomer; (**b**) comparison of the transmembrane regions of subunit B in the dimer and the rhodopsin monomer

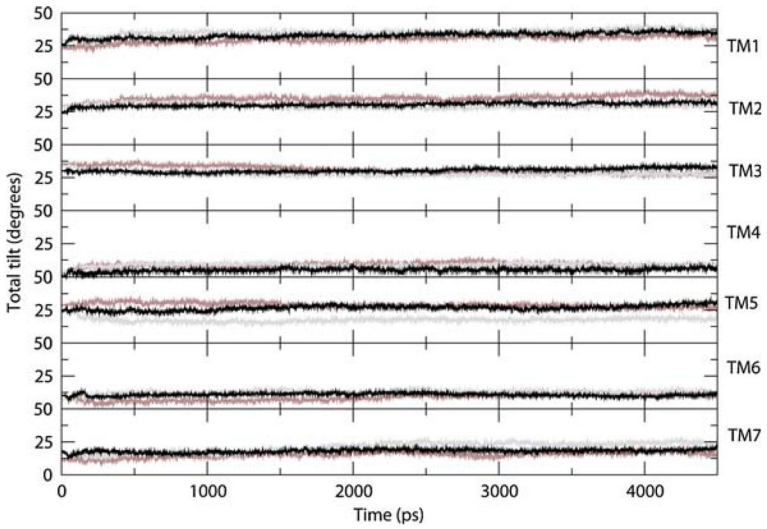

Fig. 8.

Time evolution (recorded every 10 ps) of the total tilt angle of each TM in the rhodopsin monomer (black color) and dimer (dark gray and light gray for subunits A and B, respectively) with respect to the *Z*-axis (or bilayer normal) during the 45 ns of MD simulation

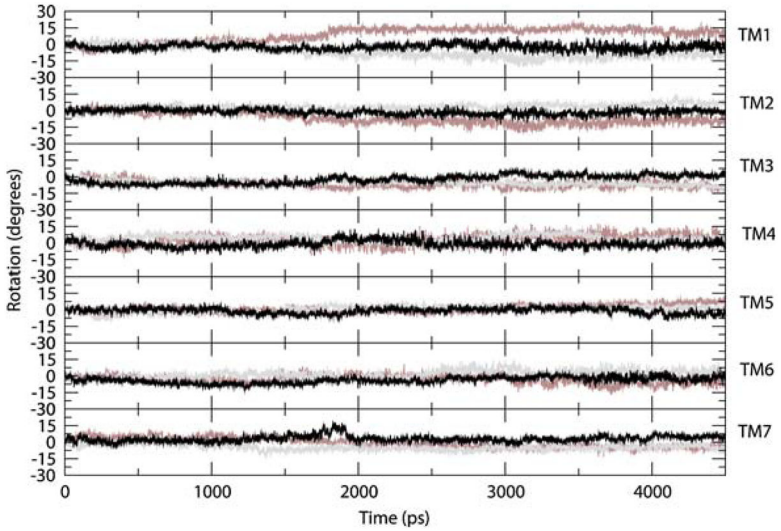

Fig. 9.

Time evolution (recorded every 10 ps) of the rotation angle of each TM in the rhodopsin monomer (black color) and dimer (dark gray and light gray for subunits A and B, respectively) around their own helical axes during the 45 ns of MD simulation

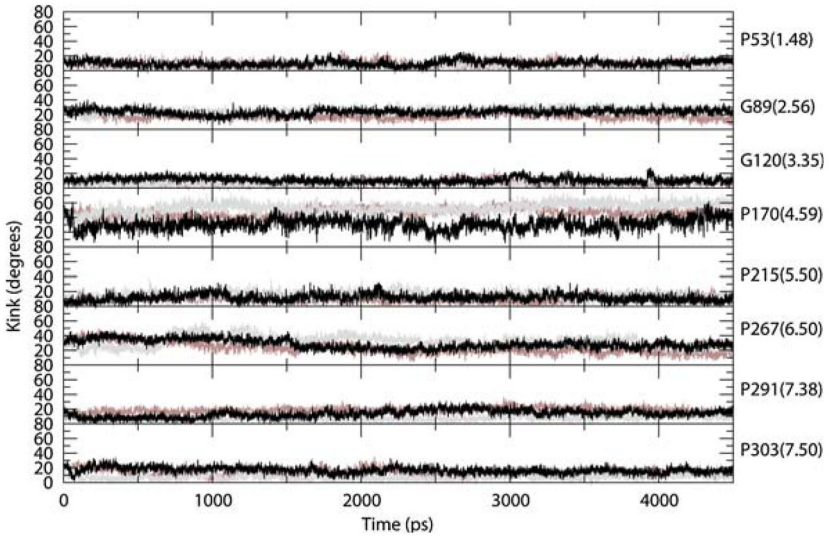

Fig. 10.

Time evolution (recorded every 10 ps during the 45 ns MD simulation) of the helical kink in TM helices of the rhodopsin monomer (black line in the figure) and dimer (dark gray and light gray for subunits A and B, respectively) that contain either a proline residue or two consecutive glycines in their interior. Specifically, kinks were centered at the following residues: P53 (1.48), G89 (2.56), G120 (3.35), P170 (4.59), P215 (5.50), P267 (6.50), P291 (7.38), and P303 (7.50)